

Subcycle Transient Scanning Tunneling Spectroscopy with Visualization of Enhanced Terahertz Near Field

Shoji Yoshida,[†] Hideki Hirori,[‡] Takehiro Tachizaki,[§] Katsumasa Yoshioka,^{||} Yusuke Arashida,[†] Zi-Han Wang,[†] Yasuyuki Sanari,[‡] Osamu Takeuchi,[†] Yoshihiko Kanemitsu,[‡] and Hidemi Shigekawa^{*,†}

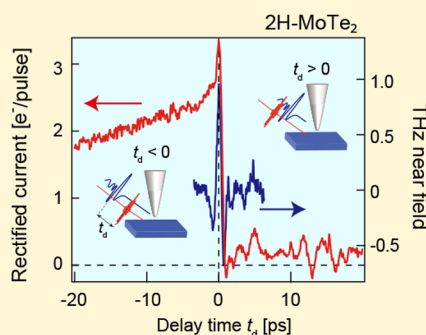
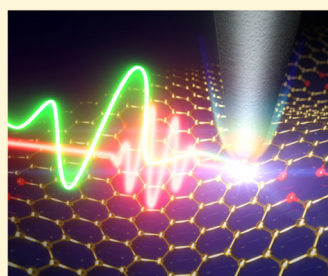
[†]Faculty of Pure and Applied Sciences, University of Tsukuba, Tsukuba 305-8573, Japan

[‡]Institute for Chemical Research, Kyoto University, Uji, Kyoto 611-0011, Japan

[§]Department of Optical and Imaging Science and Technology, Tokai University, Hiratsuka-shi, Kanagawa 259-1292, Japan

^{||}Department of Physics, Graduate School of Engineering, Yokohama National University, Yokohama, 240-8501, Japan

Supporting Information



ABSTRACT: The recent development of optical technology has enabled the practical use of a carrier-envelope phase-controlled monocycle electric field in the terahertz (THz) regime. By combining this technique with metal nanostructures such as nanotips, which induce near-field enhancement, the development of novel applications is anticipated. In particular, THz scanning tunneling microscopy (THz-STM) is a promising technique for probing ultrafast dynamics with the spatial resolution of STM. However, the modulation of the THz waveform is generally accompanied by an enhancement of the electric field, which is unknown in actual measurement environments. Here, we present a method enabling direct evaluation of the enhanced near field in the tunnel junction in THz-STM in the femtosecond range, which is essential for the use of the THz near field. In the tunneling regime, it was also demonstrated that the transient electronic state excited by an optical pulse can be evaluated using the THz-STM, and the ultrafast carrier dynamics in 2H-MoTe₂ excited by an optical pulse was reproducibly probed.

KEYWORDS: scanning tunneling microscopy, terahertz, near field, ultrafast dynamics

When a nanoscale metal structure is irradiated by electromagnetic waves, the near field formed on the material surface is enhanced in a confined space far beyond the diffraction limit.¹ With a metal probe (nanotip), it is possible to obtain an intense terahertz (THz) near field in a local region directly beneath the nanotip owing to the field enhancement effect.² Therefore, this near field not only allows THz nanoscopy of structures much smaller than the wavelength of light beyond the diffraction limit³ but also provides a platform for studying strong-field-driven dynamics.^{4,5} Furthermore, the practical use of light with a controlled carrier-envelope phase (CEP) has recently become possible. In particular, in the case of THz waves, it is possible to spontaneously obtain CEP-stable light consisting of almost monocycle pulses through optical rectification by irradiating ultrashort optical pulses to a THz antenna and various nonlinear optical crystals.⁶

The application of this technology is expected to open new research areas, such as nanodevices that coherently control tunneling currents,^{2,7} THz electron guns,^{8,9} and new measurement and processing techniques as a result of combining THz waves with near-field scanning optical microscopy (NSOM) and scanning tunneling microscopy (STM).^{2,10–15} For example, an ultrashort-pulse electron beam obtained by controlling the photoelectron emission from a metal probe in the time domain of a THz subcycle has realized new ultrafast electron microscopy, which enables the observation of ultrafast dynamics at the atomic scale.^{9,16} By irradiating the tunnel junction with THz pulses, an ultrafast tunneling current has

Received: February 14, 2019

Published: May 16, 2019

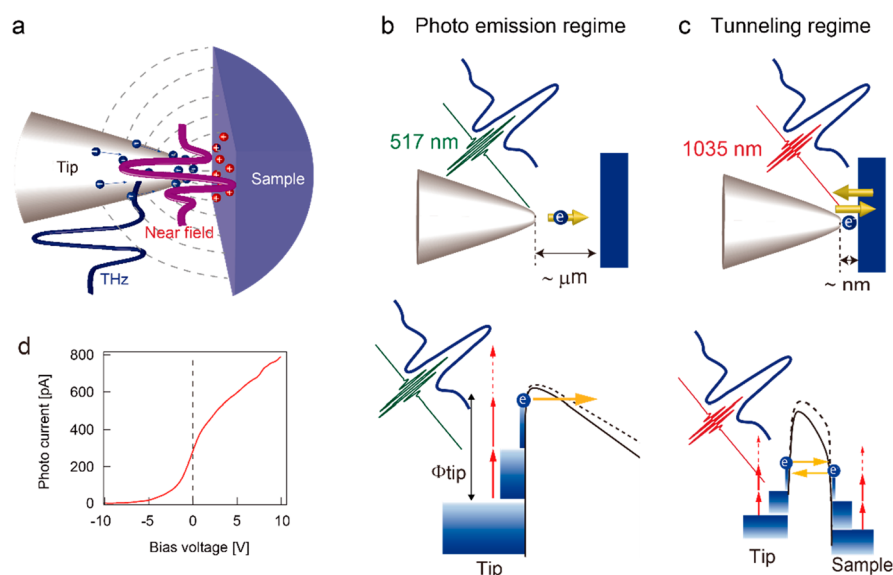


Figure 1. Explanation of measurement principle. (a) Incident electric field and its modulation by a nanotip. (b, c) Schematic illustrations of measurement methods in photoemission (photoemission and above-threshold photoemission) regime and tunneling regime, respectively. The barrier height is modulated by the THz electric field, and photoelectron emission (hot electron tunneling) is induced by the simultaneous irradiation by the probe light of 517 nm (1035 nm). (d) Dependence of photocurrent on the dc bias voltage V_{DC} applied to the HOPG sample with respect to the nanotip while the tip was irradiated by the probe light and the THz electric field was turned off. The photocurrent observed for $V_{\text{DC}} \leq 0$ was due to above-threshold photoelectron emission caused by the process of three-photon absorption.

been driven, and its direction can be coherently manipulated by changing the CEP of the THz pulse.¹⁵

Recently, THz-STM has been developed using the above-described mechanism, in which the tip-enhanced THz near field is operated as a transient tunnel voltage V_{THz} , and the THz-induced tunneling current I_{THz} is measured as a signal. Since the tip enhancement reaches a factor of 1×10^5 , it is possible to obtain the electric field strength necessary for the ultrafast driving of tunneling current with a relatively weak incident THz pulsed electric field.² In THz-STM, since the thermal expansion of the tip and sample is small,^{2,10} time-resolved measurement can be performed by measuring the current at the moment the bias voltage is applied. The carrier dynamics of optically pumped InAs nanodots and molecular orbitals of a vibrating pentacene single molecule were visualized in real space with an atomic-level locality of I_{THz} and a high temporal resolution of sub-picoseconds.^{10,11}

With the precise control and utilization of the electric field inside optical pulses, further extension toward the extreme limits of measurement and control can be expected. However, although THz electromagnetic waves are enhanced by coupling the antenna with the nanotip, as described above, the electric field waveform is also modulated simultaneously, as schematically shown in Figure 1a. This has been experimentally confirmed in NSOM and THz-STM.^{15,17} Although the theoretical description of the antenna effect and other models has been discussed,¹⁷ to realize precise measurement and control, it is essential to develop a new method for directly measuring and quantitatively evaluating the waveform in actual measurement environments.

Here, we present a new method enabling the visualization of the enhanced THz near-field waveform over a nanotip and the tunnel junction by controlling the photoelectron emission and tunneling current in the femtosecond range. In the tunneling regime, it was also demonstrated that the transient electronic state excited by an optical pulse can be evaluated using the

THz field as the instantaneous bias voltage, and the ultrafast carrier dynamics in 2H-MoTe₂ excited by an optical pulse was reproducibly probed.

RESULTS

Experimental Setup. In this study, we performed experiments using a system constructed by combining an ultrashort-pulse laser and an ultrahigh-vacuum STM system (base pressure: $<1 \times 10^{-7}$ Pa), which enables precise manipulation of the nanotip position (Figure S1). A tungsten (W) STM tip coated with PtIr was used as the nanotip for measurement. As shown in Figure 1b,c, the nanotip was irradiated with two types of optical pulses: a THz light and a probe light. The THz pulse was generated by irradiating a LiNbO₃ crystal with an infrared (IR) pulse (1035 nm, 309 fs, 1 MHz), and it was almost a monocycle with a large first peak of 1 ps width, as shown in Figure 2g. For the probe light, IR light and 517 nm light, which was generated by converting the IR light into a second-harmonic wave using a β -BaB₂O₄ (BBO) crystal, were prepared for the two types of measurements in which the photoelectron emission current (Figure 1b) and hot electron tunneling current (Figure 1c) were detected as a signal.

In a previous work, the THz near field at the metal tip apex was evaluated using the THz-field-driven photoemission (photoemission) from the nanotip.^{3,18} In our case, by using the STM setup, we realized two-dimensional (2D) analysis of the enhanced near field, including measurements in the tunnel regime. As an initial stepwise comparison, highly oriented pyrolytic graphite (HOPG), a typical material, and Bi₂Se₃, which has been well-studied by photoelectron spectroscopy,¹⁹ were used as samples. The relaxation of the excited electronic states in these materials is sufficiently fast compared with temporal oscillation of the THz electric field, enabling probing of the THz pulse waveform. In the case of the Bi₂Se₃ sample, there are fast (<1 ps) and slow (~ 10 ps) relaxation

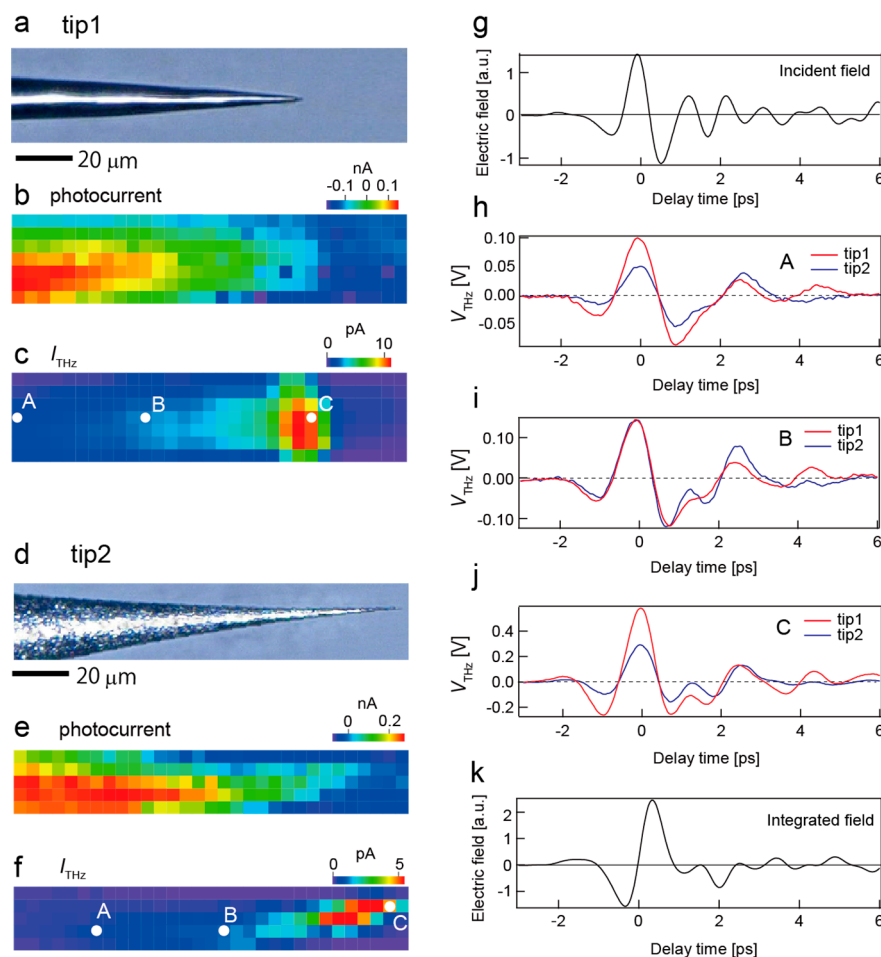


Figure 2. THz electric field modulation by nanotip. (a) Optical micrograph of the ultrasharp PtIr-coated W nanotip (tip 1). (b) Map of photoelectrons obtained by scanning the probe light (517 nm) on the nanotip. The spot position was moved by 31 steps of $4.5 \mu\text{m}$ in the x direction; then, after being shifted by $4.5 \mu\text{m}$ in the y direction, it was moved back along the x direction in 31 steps. This procedure was repeated, until seven steps had been completed in the y direction (the entire scanned area was $139.5 \times 31.5 \mu\text{m}^2$). (c) Map of I_{THz} at zero delay time. (d) Optical micrograph of the PtIr-coated W nanotip fabricated by ordinary chemical etching (tip 2). (e) Map of photoelectrons obtained by scanning the probe light (517 nm) on the nanotip. (f) Map of I_{THz} at zero delay time. (g) Waveform of the incident THz light. (h–j) THz near-field waveforms measured at A, B, and C in (c) and (f), respectively. Red and blue lines show the results for tips 1 and 2, respectively. (k) Waveform obtained by integrating the electric field in (g). $V_s = +10 \text{ V}$, $I_{\text{VIS}} = 14 \text{ mW}$, $E_{\text{THz,pk}} = 4.1 \text{ kV/cm}$ (electric field of the maximum peak), $f_{\text{rep}} = 200 \text{ kHz}$, and tip–sample distance $\approx 1000 \text{ nm}$. Here, an HOPG sample was used as the counter electrode.

components for high-energy ($E - E_F > 1 \text{ eV}$) and low-energy regions, respectively. Hot electrons excited up to the high-energy bulk and surface states are cooled to a lower state within 1 ps. Such an ultrafast response of the hot electrons allows us to probe the THz near-field waveform in the STM tunnel junction.

In the last part of this paper, we show the result of time-resolved measurement using 2H-MoTe₂ as a sample. We excited (pumped) the sample using IR light and measured the dynamics of the excited state using a THz pulse as the instantaneous bias voltage to be applied between the STM tip and sample.

Visualization of Terahertz Near-Field Waveform by Photoelectron Emission. First, we present the method and results when photoelectron emission was used for measurement. When irradiating a nanotip, photoelectron emission is induced by multiphoton absorption of the probe light (517 nm). The generated photoelectrons flow from the nanotip to an HOPG sample upon applying direct-current (dc) bias voltage V_{DC} to the sample with respect to the nanotip and are detected by a current preamplifier. Since the photoelectron

generation efficiency depends on the height of the potential barrier at the W nanotip surface, the photocurrent intensity changes with the profile of the barrier height, which is modulated by V_{DC} and the THz near field generated on the nanotip, as shown in Figure 1b.

Figure 1d shows a current–voltage (I – V) curve obtained by varying the applied sample bias voltage V_{DC} , while the tip was irradiated by the probe light with the THz electric field turned off. The photocurrent observed for $V_{\text{DC}} \leq 0$ was due to above-threshold photoelectron emission caused by the process of three-photon absorption. The photoelectron current increased monotonically as a function of V_{DC} . It was also confirmed that the THz-induced photoelectron current I_{THz} , which was generated by the bias voltage produced by the THz pulse in addition to V_{DC} , linearly changed with the incident THz field strength, $I_{\text{THz}} \propto E_{\text{THz}}$ in this bias voltage range (Figure S2). Therefore, it is considered possible to investigate a THz near-field waveform by measuring I_{THz} while varying the delay time t_d between the THz pulse and the probe pulse. To detect the weak signal, the pump laser generating the THz pulses was chopped at 430 Hz, and $I_{\text{THz}}(t_d)$ was measured by the lock-in

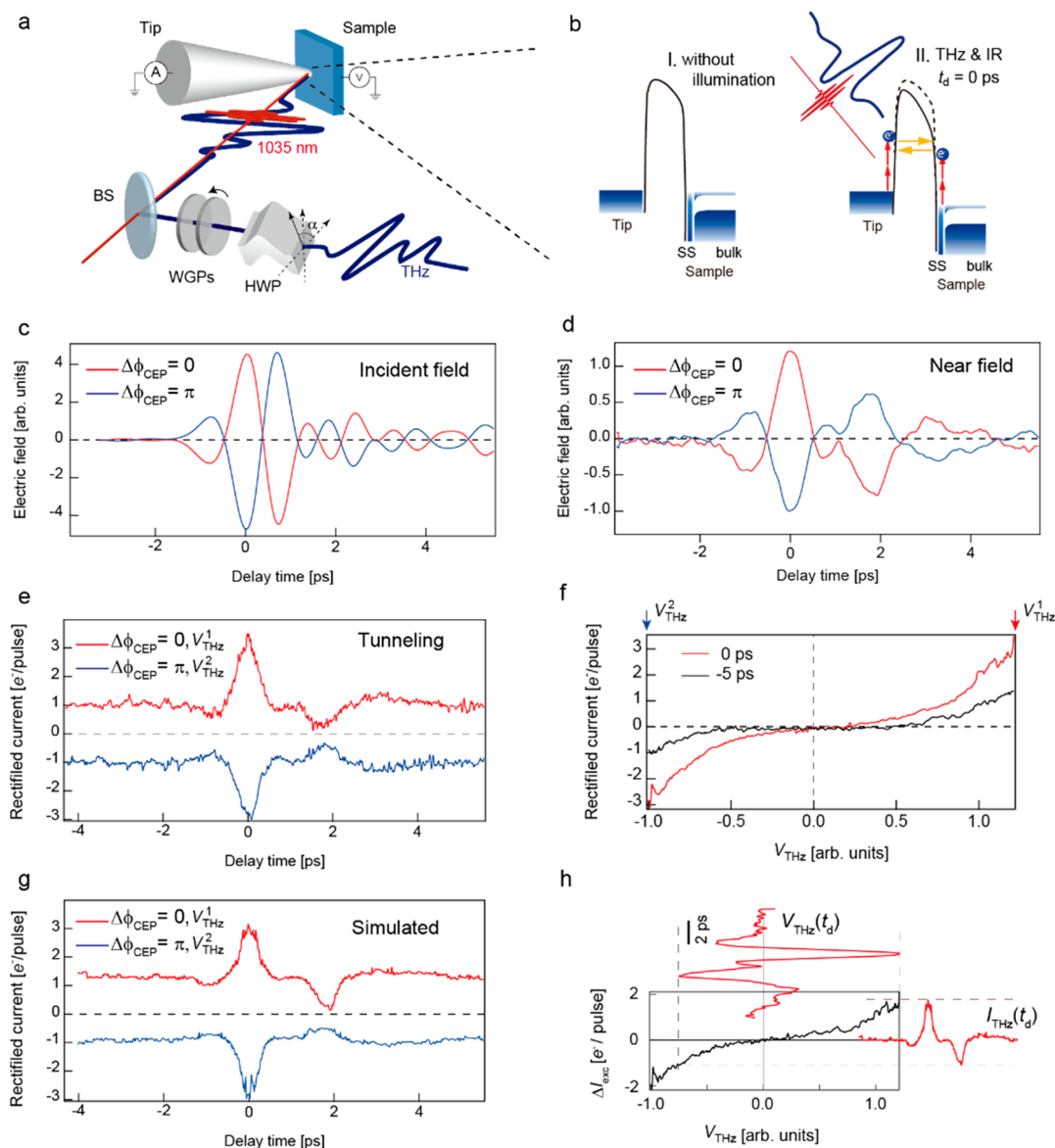


Figure 3. Measurement in tunnel regime. (a) Schematic illustration of the measurement setup. The IR pulse wavelength was set to 1035 nm. The direction of the THz pulse generated by a lithium niobate crystal was inverted by CEP control using the HWP. The THz field strength was continuously controlled using a wire grid polarizer. (b) Tunnel junction band diagrams (I) without and (II) with IR pulse and THz pulse irradiation. (c) Electrical over-stress measurement results of the incident THz waveform. By controlling the HWP angle α and adjusting the phase of the CEP, ϕ_{CEP} , the electric field waveform can be reversed. (d) Tip-enhanced near-field waveform obtained by photoelectron measurement. (e) I_{THz} as a function of delay time ($V_{\text{S}} = 2$ mV, $I_{\text{T}} = 2$ pA, $I_{\text{IR}} = 5$ mJ/cm², $f_{\text{rep}} = 0.5$ MHz). (f) $I_{\text{THz}}-V_{\text{THz}}$ curves obtained for $t_{\text{d}} = -5$ ps and 0. (g) I_{THz} as a function of delay time simulated using the $I_{\text{THz}}-V_{\text{THz}}$ curve. (h) Schematic to explain the method of simulation to obtain the spectra shown in (g). Analysis was performed for Bi₂Se₃.

detection method. The delay time was varied at a rate of 1 ps/s. All experiments were performed at room temperature.

Figure 2 shows the results obtained using an HOPG sample as the counter electrode of the nanotip. Figure 2a,d shows optical micrographs of the two types of nanotips used in this study. Both tip 1 and tip 2 were fabricated by electropolishing, but tip 1 was sharper and had a longer tapered area (see Figure S1b for more detail). The spot position of the probe light pulse was two-dimensionally scanned over the nanotip, and the $I-V$ curve (corresponding to Figure 1d) and waveform (Figure 2) measurements were performed at each pixel position.

First, we verified that the scanning system operated correctly. When an electric field is applied, the distance between the positions probed on the tip and sample affects the

measurement. Therefore, we measured the photoelectron current for $V_{\text{DC}} = 0$ at each pixel, that is, the current obtained by photoelectrons reaching the HOPG sample without a THz electric field and sample bias voltage V_{DC} (corresponding to the value at $V_{\text{DC}} = 0$ in Figure 1d). Figure 2b,e shows the results of mapping. Each map approximately reflects the shape of the nanotip, but the intensity is low at the tip apex, because the diameter of the nanotip is smaller than the light spot size. THz waveforms were obtained by measuring the THz current $I_{\text{THz}}(t_{\text{d}})$ at each pixel position while changing t_{d} and maintaining V_{DC} at +10 V. Since the photoelectron current was almost linear with respect to the voltage around $V_{\text{DC}} = +10$ V, as shown in Figure 1d, I_{THz} only depends on E_{THz} when

photoelectron emission occurs. Thus, $I_{\text{THz}}(t_d)$ provides a direct reflection of the waveform of the THz near field.

In ref 9, the strength of the incident THz field was 100 kV/cm, and the enhanced near field obtained by time-of-flight measurement was 9 MV/cm, which was much higher than the dc voltage ($V_{\text{DC}} = 30 \text{ V}/(3 \text{ mm})$). Therefore, photoelectrons were steered back to the nanotip side, and only half the shape of the THz field was not obtained. They obtained the whole shape of the THz electric field by reversing the orientation of the setup. In our case, the strength of the incident THz field was 4.1 kV/cm, and the effective bias voltage between the STM tip and sample estimated by using the I - V curve was 0.6 V, which was lower than the applied bias voltage of 10 V. In addition, by setting the tip-sample distance close to $\sim 1 \mu\text{m}$ and V_{DC} to +10 V, the strong dc electric field between the tip and sample produced a photoelectron current larger than $I_{\text{THz}}(t_d)$. Therefore, it was possible to measure the full change in the current, while the THz electric field direction was changed from the nanotip to the sample and vice versa.

Figure 2h-j shows the THz near-field profiles obtained for the two types of nanotips by performing measurements at A, B, and C in Figure 2c,f, respectively. On the one hand, when measuring the THz waveform, V_{DC} was fixed at +10 V. On the other hand, as shown by the I - V curve in Figure 1d, the photocurrent changed almost linearly with the voltage in the vicinity of $V_{\text{DC}} = +10 \text{ V}$. Therefore, from the slopes (dI/dV) of the photoelectron I - V curves obtained at each point for $V_{\text{DC}} = +10 \text{ V}$, it was possible to convert each waveform to an effective THz voltage V_{THz} using the relationship of $dI/dV = I_{\text{THz}}/V_{\text{THz}}$, which is plotted on the vertical axis of each figure. Figure 2c,f shows maps of I_{THz} at zero delay time for tips 1 and 2, respectively. At the tip apex C, the peak values of V_{THz} for both tips were larger than those at A and B owing to the enhancement effect of the nanotip; in particular, the peak value was approximately twice as large for tip 1. Figure 2g shows the incident THz waveform obtained by electro-optic (EO) sampling (see Figure S1). In the simple model of antenna theory, the electric field generated by nanotip enhancement is obtained by integrating the original electric field,¹⁷ which is shown in Figure 2k. However, as shown in the figures, the measured waveform is different from the calculated one, emphasizing the importance of directly measuring the modulated electric field (see Figures S3 and S4 for more detail). By using STM tips with different tapering, it was shown that the near-field waveforms generated at the two different types of tips were different, even for the same incident THz electric field. Recently, this tip dependence has been more clearly observed using various tips of different shapes.¹⁵

These results indicate that it is essential to directly evaluate the near field in the actual measurement environment to obtain a deeper understanding of the phenomena and for the practical use of THz techniques.

Measurement of THz Near-Field Waveform in the Tunnel Regime. We showed that the modulation of the electric field can be characterized using the photoelectronic emission. On the one hand, depending on various parameters such as the nanotip-sample distance, vacuum barrier height, THz field strength, and optical excitation energy, we can theoretically consider the regimes of photoelectronic emission, field emission, and tunneling;^{9,18} however, this has not been sufficiently confirmed experimentally. On the other hand, since the present setup employs an STM system, measurement in the tunnel regime is possible. In the measurement by THz-

STM with electronic control by an electric field, evaluation of the electric field waveform under the measurement conditions becomes indispensable. To proceed, we used the probe that yielded the near-field profile of the tip (through the photoelectronic emission) to perform the measurement in the tunnel regime, that is, THz-STM measurement.

Figure 3a shows a schematic illustration of the experimental setup. V_{DC} and the current were set to 2 mV and 2 pA, respectively, to bring the nanotip closer to the tunnel region. The bias voltage was set to this low value instead of increasing the current to avoid the possibility of the sample breaking when the current increases. To suppress photoelectron emission, the original IR light (1035 nm) was used for the probe. When the tip was retracted 100 nm, the signal, which was observed in the range of 100 μm for the case of photoelectrons, disappeared, thus confirming that the signal originated from the tunnel current. HOPG and Bi_2Se_3 were used as samples. The signal was significantly weaker for HOPG, approximately 1/100 of that for Bi_2Se_3 , and a detailed analysis shown in Figure 3 was performed for Bi_2Se_3 (see Figure S5 and its caption for more detail). The Bi_2Se_3 sample was prepared by cleavage in vacuum.

Figure 3b shows schematic illustrations of the measurement mechanism in the tunnel regime, (I) without and (II) with irradiation. Bi_2Se_3 used for the analysis has a narrow band gap of $\sim 0.2 \text{ eV}$ in the bulk,¹⁹ and a metallic surface state called a Dirac cone is formed because of its topological property. Since Bi_2Se_3 is a degenerate n-type semiconductor owing to Se vacancies, the Fermi level is located above the bulk conduction band minimum.²⁰ Therefore, although downward band bending occurs at the surface, it is not modulated by optical excitation because of the metallic characteristics of Bi_2Se_3 .

Here, the tunnel current was measured instead of photoelectrons, which were observed for Figure 2. To detect the weak signal of the THz-induced tunnel current, the IR pulse used for THz generation was chopped at 430 Hz, and $I_{\text{THz}}(t_d)$ was measured by the lock-in detection method, as was performed for the photoelectron measurement. If an IR light pulse is irradiated while the tunnel barrier is changed owing to THz pulse irradiation, hot electrons are produced and enhance the tunnel current I_{THz} , where I_{THz} depends on the delay time between the IR pulse and the THz pulse [Figure 3b, (II)]. Since the relaxation of hot electrons in a high-energy state occurs faster than the oscillation of the THz electric field, the delay time dependence of I_{THz} was expected to represent a THz near-field waveform similar to that obtained by photoelectron emission measurement; however, the non-linearity of the I - V curve affects the spectrum, which will be discussed later.

To probe the photoexcited electronic state, the V_{THz} dependence of I_{THz} was measured with the delay time t_d fixed to zero. For this purpose, a $\lambda/2$ wave plate (HWP) for the THz range and a wire grid polarizer (WGP) were introduced in this experiment, which enabled V_{THz} to be continuously changed in both the positive and negative voltage ranges.^{15,21} When the angle of the HWP, α , shown in Figure 3a, is rotated by $\pi/2$, the phase of the CEP, ϕ_{CEP} , changes by π , and the direction of the electric field is reversed.

Figure 3c shows the waveform of the incident THz pulse measured at HWP angles of $\alpha = 0$ and $\alpha = \pi$. The THz waveform was inverted vertically as expected. Thereby, the near-field waveform at the tip apex was also inverted, as shown in Figure 3d. These near fields worked as the transient bias

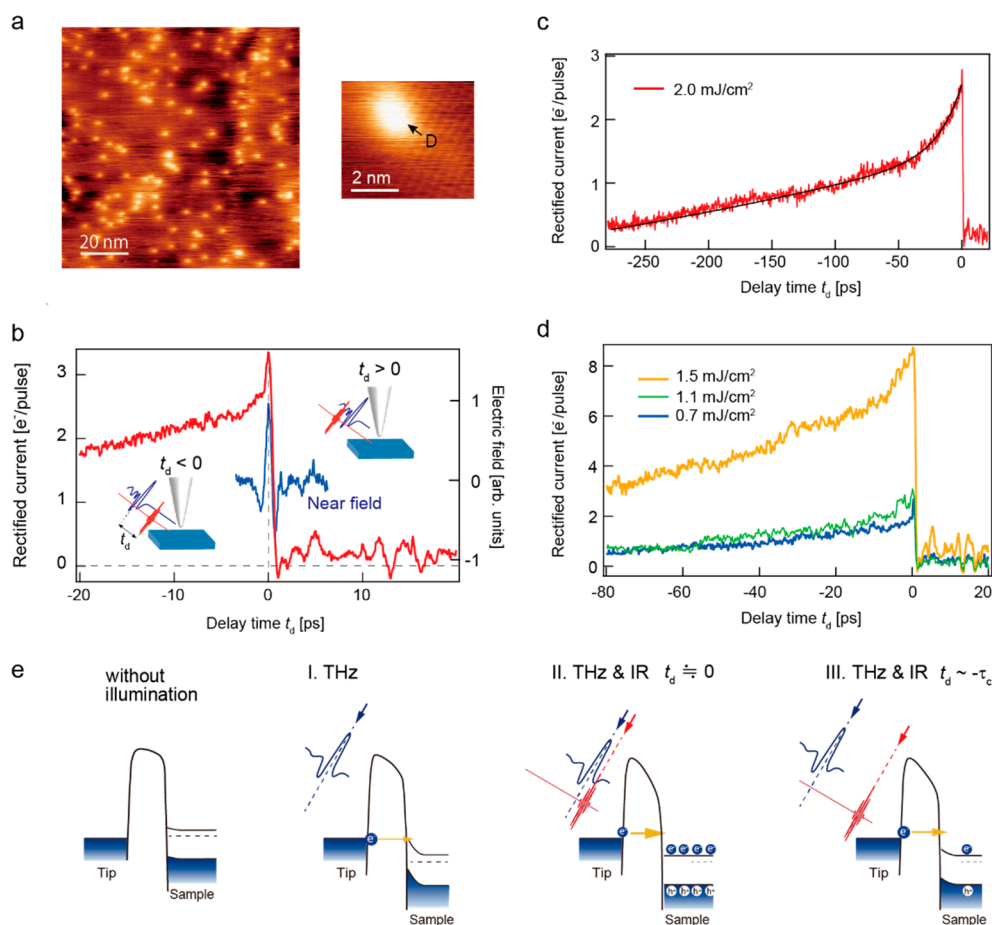


Figure 4. Transient electronic dynamics obtained by THz-STM for 2H-MoTe₂. (a) STM image of the sample (sample bias $V_S = 1.2$ V, tunnel current $I_t = 10$ pA). Bright spots indicated by D in the magnified image are defects. (b) Delay-time dependence of I_{THz} (red line). Near-field waveform at the STM tip apex used for measurement, which was obtained by the photoelectron method (blue line) is superimposed. (insets) The relationship between the pump and probe lights for $t_d < 0$ and $t_d > 0$. (c) Example of spectrum obtained over a wide delay-time range. The black line is a fitting curve with an exponential function of two components. (d) Light-intensity dependence of I_{THz} . I_{THz} has two components at 1.5 mJ/cm², but a one-component fitting is in good agreement with I_{THz} at 1.1 and 0.7 mJ/cm². ($V_S = -3$ mV, $I_T = 0.6$ pA, $f_{\text{rep}} = 1$ MHz). (e) Schematic illustrations of (left) without illumination, (I) THz illumination without IR, (II) THz illumination just after IR excitation, and (III) THz illumination after IR excitation with rather large t_d in the range of τ_c (carrier recombination lifetime).

voltages of V_{THz}^1 ($\Delta\phi_{\text{CEP}} = 0$) and V_{THz}^2 ($\Delta\phi_{\text{CEP}} = \pi$) applied to the tunnel junction. Since the tip was different from those shown in Figure 2, the waveform was slightly different from those shown in the figures. However, a common feature is that the near-field waveform is modified from the incident THz waveform. The strength of the near field shown in Figure 3d is slightly asymmetric, which may be due to the slight change in the spot position while changing the angle. However, a linear relationship was obtained between the strength of the incident THz field and that of the obtained near field (see Figure S6).

Next, the delay time dependence of I_{THz} induced by these two near-field waveforms was measured in the tunnel region, and the results are shown in Figure 3e. Measurements were performed for $V_{\text{THz}} = V_{\text{THz}}^1$ and V_{THz}^2 . The THz-pulse-induced tunnel current I_{THz} flowed from the sample to tip when $\alpha = 0$ and from the tip to the sample when $\alpha = \pi/2$, but a spectral shape similar to the near-field waveform was obtained. The fact that a delay time dependence of I_{THz} was observed implies that the tunneling probability transiently changed with the change in the electronic state induced by the IR pulse irradiation. To confirm this effect, transient I - V curve measurements were

performed for $t_d = -5$ ps and 0 by measuring I_{THz} while continuously sweeping V_{THz} by rotating the WGP and HWP.

The obtained results are shown in Figure 3f. Since the transient I - V curve for $t_d = -5$ ps represents the transient electronic state 5 ps after IR excitation, where the photoexcited state of both the tip and sample are almost completely relaxed, the shape of the transient I - V curve is considered to be similar to that of the static I - V curve without the effect of the optical pulse (Figure S7). In fact, a semiconducting electronic state was obtained. In contrast, the slope of the I - V curve increased for the case of $t_d = 0$, and the I - V curve became similar to that for a metallic electronic structure. As shown in the band diagram (II) in Figure 3b, this change corresponds to the reduction of the effective vacuum barrier by the excitation of hot electrons; the I - V curve reflects the optically excited transient electronic state.

By using the ultrafast electronic response in the tunnel junction, we can evaluate the electric field waveform by the tunnel current. The transient I - V curve depends on the delay time in accordance with the dynamics of the photoexcited electronic state. Since the relaxation of the hot electrons was fast, the excited state was almost relaxed at $t_d = -5$ ps, and

$\Delta I_{\text{exc}}(V_{\text{THz}}) [=I_{\text{THz}}(V_{\text{THz}}, 0 \text{ ps}) - I_{\text{THz}}(V_{\text{THz}}, -5 \text{ ps})]$ corresponds to the change in the I - V curve owing to photoexcitation. Therefore, $I_{\text{THz}}(t_d)$ shown in Figure 3g was simulated from the relationship shown in Figure 3h, with the near field being considered to be the voltage applied between the probe and sample. (See Figure S8 for more detail.) Unlike the case of photoelectrons, the time-resolved waveform measured by the tunneling current has a different form from the near-field waveform, because the I - V curve is nonlinear.

The peak around $t_d = 0$ is slightly wider in the experimental curve than in the simulated curve. This is thought to be due to the relaxation time of hot electrons not being taken into consideration in the simulation. It is considered that we can measure the relaxation process of hot electrons by measuring the delay-time dependence of the transient I - V curve in more detail, which is difficult at present. Since the THz near-field waveform has a tail of over 1 ps in the region of $t_d < 0$, the response of an electronic state with a similar relaxation time cannot be measured separately from the effect of the tail. It is expected to be possible to evaluate the excited state of a sample by conducting experiments using light pulses and THz pulses of a shorter time width in the future.

In addition, as clearly shown in Figure 3e, the waveform obtained by the tunnel current has a large positive–negative asymmetry (e.g., the ratio between the intensities of the first and second peaks) compared with the waveforms obtained by photoelectron emission shown in Figure 2. This is because the THz near field itself has positive–negative asymmetry, as shown in Figure 3d, and the tunnel current induced by the near field is further rectified (the asymmetry is enhanced) by the nonlinearity in the I - V curve, as schematically shown in Figure 3h. Although accurate characterization of the THz waveform with the tunnel current requires a correction using the I - V curve, as shown here, it was confirmed that the THz near-field profile can be observed even in the tunnel current regime.

As has been shown, transient I - V measurement is potentially a very powerful technique for elucidating the excited electronic states and dynamics of materials with atomic spatial resolution. For this purpose, it is indispensable to evaluate the tip-enhanced near field waveform. Since the tip-enhanced near field can be changed by adjusting the experimental conditions, environmental conditions, and the shape of the tip, it is extremely important to directly confirm the near-field waveform using the method described in this paper, in addition to by simulation such as by the finite difference time domain (FDTD) method.

Measurement of Time-Resolved Signal using THz Near Field as a Bias Voltage. In the last part, we show the result of time-resolved measurement using 2H-MoTe₂ for a sample. We excited (pumped) the sample using IR light and measured the dynamics of the excited state using the THz electric field as the instantaneous bias voltage applied between the STM tip and sample. The bulk 2H-MoTe₂ used in this study has an indirect band structure, but since it has direct band gap of 1.1 eV at the k point,²² it is possible to induce the optical transition with the IR laser of our system (1035 nm).

Figure 4 shows the experimental scheme and a typical result. Figure 4a shows an STM image of the sample surface. The bright spots observed in the image are attributed to intrinsic defects such as vacancies.²³ Figure 4b shows the delay-time dependence of I_{THz} (red line). The enhanced near field of the THz probe pulse used for measurement, whose waveform was

evaluated by the photoelectron method (blue line), is superimposed. The insets show the relationship between the pump and probe lights for $t_d < 0$ and $t_d > 0$. On the one hand, for $t_d > 0$, similar to the case of Bi₂Se₃, the THz near-field waveform was observed through the fast response of the sample such as hot electrons, although the signal was small. On the other hand, for $t_d < 0$, since the THz pulse was irradiated after the IR pulse, as shown in the inset, I_{THz} reflects the dynamics of the excited state due to photocarrier generation. Since 2H-MoTe₂ is a conventional semiconductor, in contrast to Bi₂Se₃, photocarriers excited by optical pulses induce a surface photovoltage,^{24,25} leading to a change in I_{THz} . Thus, the delay-time dependence of I_{THz} for $t_d < 0$ represents the carrier decay process in 2H-MoTe₂. Figure 4e illustrates energy band diagrams of the STM tunneling junction in the steady state (without illumination) and the THz pulse-induced non-equilibrium state at the peak of the THz field (I–III). In the nonequilibrium state, when both THz and IR pulse illuminate the tunnel junction, photocarriers generated by IR pulse screen the THz field in semiconductor, and THz field is fully applied to the vacuum gap, as shown in II. Without photocarriers, THz near field partially penetrates the semiconductor surface and induces surface band bending shown in I, which reduces effective THz field applied to the vacuum gap and suppresses I_{THz} . Therefore, in the case of III, I_{THz} decreases as t_d becomes longer where photocarriers were decreases due to carrier recombination.

Figure 4c shows the results of measurement over a wide delay-time range, focusing on the $t_d < 0$ side. Because of the limited range of the delay time, the appearance of the entire long decay component was not clear. Here, we assumed a simple model, and the relaxation of the excited state was well-fitted with a two-component exponential function with the lifetimes of $\tau_{\text{fast}} = 18 \text{ ps}$ and $\tau_{\text{slow}} = 606 \text{ ps}$. On the one hand, τ_{slow} , which was considered to be the carrier recombination lifetime, was also confirmed by optical pump–probe measurement.²² On the other hand, the fast relaxation time τ_{fast} appeared when the pump fluence was increased more than 1.5 mJ/cm² as shown in light intensity dependence (Figure 4d). The result suggests that the fast carrier recombination was due to the capture of electrons and holes by defects via Auger processes, as was observed in other transition-metal dichalcogenide monolayer (TMDC) materials,²⁶ because the mechanism is dominant when the photocarrier density is high.²⁷ Since the signal originated from the hot electrons in the case of the Bi₂Se sample, the conductance increased for positive and negative bias voltages to give similar results. In the case of 2H-MoTe, since band bending and other surface characteristics are involved, the bias-voltage dependence of signal may become more complicated. We leave a detailed analysis to future work.

CONCLUSION

The combination of CEP-controlled monocycle pulses in the THz regime with metal nanostructures such as nanotips has interesting novel applications, which require a precise understanding of the THz waveform. However, when a THz electric field is irradiated to a nanostructure, the electric field is amplified, although its waveform is also modulated. Therefore, it is urgently necessary to develop a new method to directly measure and evaluate near-field waveforms in actual measurement environments.

We have succeeded in developing a new spectroscopy technique capable of visualizing the spatially resolved THz near field at a nanotip by controlling the photoelectron emission from the nanotip with subcycle time resolution. In addition, using the STM system in our experimental setup, we successfully demonstrated that the waveform can also be observed in the tunnel regime. In the tunnel regime, it was demonstrated that the transient electronic state excited by an optical pulse can be measured using the THz field as the instantaneous bias voltage. The ultrafast carrier dynamics in 2H-MoTe₂ excited by an optical pulse was reproducibly probed.

Considering the rapid development of current research on the measurement and control of the extreme quantum limit via light, CEP technology will be a key to obtaining a deeper understanding of quantum processes and for the development of new devices such as to investigate the dynamics of hot electrons²⁸ and spins^{29–32} and to perform single-molecule measurement,^{33,34} for example. Our method, which enables the evaluation and accurate control of the CEP, is thus expected to play an essential role in the further advancement of science and technology.

■ ASSOCIATED CONTENT

Supporting Information

The Supporting Information is available free of charge on the ACS Publications website at DOI: 10.1021/acsphtonic.9b00266.

Schematic of experimental setup, data plots showing dependence of THz waveform at tip apex on electric field strength, frequency dependence of THz electric field modulated by the two types of nanotips, FDTD simulations of near field, measurement results for HOPG, relationship between tip-enhanced near field strength and THz intensity, tunnel spectrum of Bi₂Se₃, tip-sample distance dependence of the near-field waveform at the tip apex (PDF)

■ AUTHOR INFORMATION

Corresponding Author

*E-mail: hidemi@bk.tsukuba.ac.jp.

ORCID

Yoshihiko Kanemitsu: 0000-0002-0788-131X

Hidemi Shigekawa: 0000-0001-9550-5148

Author Contributions

S.Y., H.H., and T.T. contributed equally to this research by advancing the THz-STM system and performing experiments. K.Y. contributed to the transient spectroscopy measurement, and FDTD simulations were performed by H.H., T.T., and Y.S., while Z.W. performed OPP measurement for comparison. Y. A., O. T. and Y.K. provided technical advice. H.S. organized and supervised the project and edited the paper with S.Y. and the other authors.

Notes

The authors declare no competing financial interest.

■ ACKNOWLEDGMENTS

H.S. and T.T. acknowledge the financial support of a Grant-in-Aid for Scientific Research (17H06088 and 19H02562, respectively) from Japan Society for the Promotion of Science. H.H. acknowledges the financial support of PRESTO (No.

JPMJPR1427) grants from JST and Murata Science Foundation. We thank Y. Kawada, H. Takahashi, and Hamamatsu Photonics K. K. for fabricating the achromatic terahertz quarter-wave plate.

■ REFERENCES

- (1) Betzig, E.; Trautman, J. K. Near-Field Optics: Microscopy, Spectroscopy, and Surface Modification Beyond the Diffraction Limit. *Science* **1992**, *257*, 189–195.
- (2) Yoshioka, K.; Katayama, I.; Minami, Y.; Kitajima, M.; Yoshida, S.; Shigekawa, H.; Takeda, J. Real-Space Coherent Manipulation of Electrons in a Single Tunnel Junction by Single-Cycle Terahertz Electric Fields. *Nat. Photonics* **2016**, *10*, 762–765.
- (3) Huber, A. J.; Keilmann, F.; Wittborn, J.; Aizpurua, J.; Hillenbrand, R. Terahertz Near-Field Nanoscopy of Nanodevices. *Nano Lett.* **2008**, *8*, 3766–3770.
- (4) Herink, G.; Solli, D. R.; Gulde, M.; Ropers, C. Field-Driven Photoemission from Nanostructures Quenches the Quiver Motion. *Nature* **2012**, *483*, 190–193.
- (5) Sanari, Y.; Tachizaki, T.; Saito, Y.; Makino, K.; Fons, P.; Kolobov, A. V.; Tominaga, J.; Tanaka, K.; Kanemitsu, Y.; Hase, M.; Hirori, H. Zener Tunneling Breakdown in Phase-Change Materials Revealed by Intense Terahertz Pulses. *Phys. Rev. Lett.* **2018**, *121*, 165702.
- (6) Hirori, H.; Doi, A.; Blanchard, F.; Tanaka, K. Single-Cycle Terahertz Pulses with Amplitudes Exceeding 1 MV/cm Generated by Optical Rectification in LiNbO₃. *Appl. Phys. Lett.* **2011**, *98*, 091106.
- (7) Rybka, T.; Ludwig, M.; Schmalz, M. F.; Knittel, V.; Brida, D.; Leitenstorfer, A. Sub-Cycle Optical Phase Control of Nanotunnelling in the Single-Electron Regime. *Nat. Photonics* **2016**, *10*, 667–670.
- (8) Li, S.; Jones, R. R. High-Energy Electron Emission from Metallic Nano-Tips Driven by Intense Single-Cycle Terahertz Pulses. *Nat. Commun.* **2016**, *7*, 13405.
- (9) Wimmer, L.; Herink, G.; Solli, D. R.; Yalunin, S. V.; Echternkamp, K. E.; Ropers, C. Terahertz Control of Nanotip Photoemission. *Nat. Phys.* **2014**, *10*, 432–436.
- (10) Cocker, T. L.; Jelic, V.; Gupta, M.; Molesky, S. J.; Burgess, J. A. J.; Reyes, G. D. L.; Titova, L. V.; Tsui, Y. Y.; Freeman, M. R.; Hegmann, F. A. An Ultrafast Terahertz Scanning Tunnelling Microscope. *Nat. Photonics* **2013**, *7*, 620–625.
- (11) Cocker, T. L.; Peller, D.; Yu, P.; Repp, J.; Huber, R. Tracking the Ultrafast Motion of a Single Molecule by Femtosecond Orbital Imaging. *Nature* **2016**, *539*, 263–267.
- (12) Eisele, M.; Cocker, T. L.; Huber, M. a.; Plankl, M.; Viti, L.; Ercolani, D.; Sorba, L.; Vitiello, M. S.; Huber, R. Ultrafast Multi-Terahertz Nano-Spectroscopy with Sub-Cycle Temporal Resolution. *Nat. Photonics* **2014**, *8*, 841–845.
- (13) Jelic, V.; Iwaszczuk, K.; Nguyen, P. H.; Rathje, C.; Hornig, G. J.; Sharum, H. M.; Hoffman, J. R.; Freeman, M. R.; Hegmann, F. A. Ultrafast Terahertz Control of Extreme Tunnel Currents through Single Atoms on a Silicon Surface. *Nat. Phys.* **2017**, *13*, 591–597.
- (14) Shigekawa, H.; Yoshida, S.; Takeuchi, O. Nanoscale Terahertz Spectroscopy. *Nat. Photonics* **2014**, *8*, 815–817.
- (15) Yoshioka, K.; Katayama, I.; Arashida, Y.; Ban, A.; Kawada, Y.; Konishi, K.; Takahashi, H.; Takeda, J. Tailoring Single-Cycle Near Field in a Tunnel Junction with Carrier-Envelope Phase-Controlled Terahertz Electric Fields. *Nano Lett.* **2018**, *18*, 5198–5204.
- (16) Kealhofer, C.; Schneider, W.; Ehberger, D.; Ryabov, A.; Krausz, F.; Baum, P. All-Optical Control and Metrology of Electron Pulses. *Science* **2016**, *352*, 429–433.
- (17) Wang, K.; Mittleman, D. M.; Van Der Valk, N. C. J.; Planken, P. C. M. Antenna Effects in Terahertz Apertureless Near-Field Optical Microscopy. *Appl. Phys. Lett.* **2004**, *85*, 2715–2717.
- (18) Herink, G.; Wimmer, L.; Ropers, C. Field Emission at Terahertz Frequencies: AC-Tunneling and Ultrafast Carrier Dynamics. *New J. Phys.* **2014**, *16*, 123005.
- (19) Sobota, J. A.; Yang, S.; Analytis, J. G.; Chen, Y. L.; Fisher, I. R.; Kirchmann, P. S.; Shen, Z. X. Ultrafast Optical Excitation of a

Persistent Surface-State Population in the Topological Insulator Bi_2Se_3 . *Phys. Rev. Lett.* **2012**, *108*, 117403.

(20) Bahramy, M. S.; King, P. D. C.; de la Torre, a.; Chang, J.; Shi, M.; Patthey, L.; Balakrishnan, G.; Hofmann, P.; Arita, R.; Nagaosa, N.; et al. Emergent Quantum Confinement at Topological Insulator Surfaces. *Nat. Commun.* **2012**, *3*, 1157–1159.

(21) Kawada, Y.; Yasuda, T.; Takahashi, H. Carrier Envelope Phase Shifter for Broadband Terahertz Pulses. *Opt. Lett.* **2016**, *41*, 986–989.

(22) Chen, K.; Roy, A.; Rai, A.; Movva, H. C. P.; Meng, X.; He, F.; Banerjee, S. K.; Wang, Y. Accelerated Carrier Recombination by Grain Boundary/Edge Defects in MBE Grown Transition Metal Dichalcogenides. *APL Mater.* **2018**, *6*, 056103.

(23) Guguchia, Z.; Uemura, Y. J.; Pasupathy, A. N.; Edelberg, D.; Shermadini, Z.; Billinge, S. J. L.; Kerelsky, A.; Morenzoni, E.; Shengelaya, A.; Augustin, M.; et al. Magnetism in Semiconducting Molybdenum Dichalcogenides. *Sci. Adv.* **2018**, *4*, No. eaat3672.

(24) Terada, Y.; Yoshida, S.; Takeuchi, O.; Shigekawa, H. Real-Space Imaging of Transient Carrier Dynamics by Nanoscale Pump-Probe Microscopy. *Nat. Photonics* **2010**, *4*, 869–874.

(25) Mogi, H.; Kikuchi, R.; Yoshida, S.; Takeuchi, O.; Shigekawa, H.; et al. Externally Triggerable Optical Pump-Probe Scanning Tunneling Microscopy. *Appl. Phys. Express* **2019**, *12*, 025005.

(26) Wang, H.; Zhang, C.; Chan, W.; Tiwari, S.; Rana, F. Ultrafast Response of Monolayer Molybdenum Disulfide Photodetectors. *Nat. Commun.* **2015**, *6*, 17–20.

(27) Kar, S.; Su, Y.; Nair, R. R.; Sood, A. K. Probing Photoexcited Carriers in a Few-Layer MoS_2 Laminate by Time-Resolved Optical Pump-Terahertz Probe Spectroscopy. *ACS Nano* **2015**, *9*, 12004–12010.

(28) Wu, S. W.; Ogawa, N.; Ho, W. Atomic-Scale Coupling of Photons to Single-Molecule Junctions. *Science* **2006**, *312*, 1362–1365.

(29) Wang, Z.; Yoon, C.; Yoshida, S.; Arashida, Y.; Takeuchi, O.; Ohno, Y.; Shigekawa, H. Surface-Mediated Spin Dynamics Probed by Optical-Pump-Probe Scanning Tunneling Microscopy. *Phys. Chem. Chem. Phys.* **2019**, *21*, 7256.

(30) Loth, S.; Etzkorn, M.; Lutz, C. P.; Eigler, D. M.; Heinrich, A. J. Measurement of Fast Electron Spin Relaxation Times with Atomic Resolution. *Science* **2010**, *329*, 1628–1630.

(31) Krause, S.; Sonntag, A.; Hermenau, J.; Friedlein, J.; Wiesendanger, R. High-Frequency Magnetization Dynamics of Individual Atomic-Scale Magnets. *Phys. Rev. B: Condens. Matter Mater. Phys.* **2016**, *93*, 064407.

(32) Yoshida, S.; Aizawa, Y.; Wang, Z. H.; Oshima, R.; Mera, Y.; Matsuyama, E.; Oigawa, H.; Takeuchi, O.; Shigekawa, H. Probing Ultrafast Spin Dynamics with Optical Pump-Probe Scanning Tunneling Microscopy. *Nat. Nanotechnol.* **2014**, *9*, 588–593.

(33) Li, S.; Chen, S.; Li, J.; Wu, R.; Ho, W. Joint Space-Time Coherent Vibration Driven Conformational Transitions in a Single Molecule. *Phys. Rev. Lett.* **2017**, *119*, 176002.

(34) Yoshida, S.; Taninaka, A.; Sugita, Y.; Katayama, T.; Takeuchi, O.; Shigekawa, H. Revealing the Conformational Dynamics in a Single-Molecule Junction by Site- and Angle-Resolved Dynamic Probe Method. *ACS Nano* **2016**, *10*, 11211–11218.